# Complete single-ionization momentum spectra for strong perturbation collisions

R. E. Olson and C. J. Wood
*Department of Physics, University of Missouri-Rolla, Rolla, Missouri 65401*

H. Schmidt-Böcking
*Institut für Kernphysik, University of Frankfurt, D-60486 Frankfurt/Main, Germany*

R. Moshammer and J. Ullrich
*Universität Freiburg, Fakultät für Physik, D-79104 Freiburg, Germany*
(Received 11 August 1997)

The combination of recoil ion and ionized electron momentum spectroscopy provides an unparalleled method to investigate the details of ion-atom collision dynamics in kinematically complete experiments. To predict single ionization scattering behavior at the level now realized by experiment, the classical trajectory three-body Monte Carlo method has been used to obtain complete momenta information for the ionized electron, recoil ion, and projectile in the collision plane defined by the incident projectile and outgoing recoil ion. Strongly coupled systems were considered where the charge state of the projectile divided by the speed of the collision $q/v$ is greater than unity. Illustrated are 3.6-MeV/nucleon $Se^{28+}$ and 9.5-MeV/nucleon $Ni^{26+}$ collisions on He where experimental data are available. The theoretical results are in good agreement with these data and calculations have been performed for 165-keV/nucleon and 506-keV/nucleon $C^{6+}+He$ to compare results for the same $q/v$ perturbation strengths, but at much lower velocities. In all cases the ejected electrons are found to be preferentially emitted opposite to the recoil ion in the projectile-recoil collision plane. The 165-keV/nucleon $C^{6+}$ spectra are especially rich in that electron capture strongly contributes to the overall electron loss process. Here, the electron capture to the continuum (ECC) spectrum is observed to have not only the known asymmetry in the longitudinal direction, but also has an almost complete asymmetry in the collision plane opposite to the recoil ion. Collision plane spectra differential in the transverse momenta of the recoil ion depict the transition from soft electrons for low transverse recoil momenta, to two-center, and ECC electrons for increasing transverse recoil ion momenta. [S1050-2947(98)10006-9]

PACS number(s): 34.50.Fa, 34.10.+x

## I. INTRODUCTION

The experimental application of recoil ion momentum spectroscopy has rapidly matured in the last decade. Originally, recoil ions were used as a source of slow, multiply charged ions that were then employed in subsequent collision measurements. Studies were also made of the average energies of the recoil ions as a function of charge state. However, by the 1980s, the first measurements were being made on the transverse momentum distributions of recoil ions. These early momentum measurements were severely limited by the thermal motion of the target atoms, which markedly restricted the precision of the observations (see Ref. [1] for a review).

The development of ''cold'' targets and position-sensitive detection has removed many of the impediments of the method (see Ref. [2] for a detailed description of the method). As examples, Dörner *et al.* [3] displayed the interplay of three-body collision dynamics for $H^+ + He$ single ionization collisions by comparing recoil ion transverse momenta against projectile scattering angle. The Kansas State group lead by Cocke used recoil ion spectroscopy to measure the $Q$ values for electron transfer collisions [4,5] and clearly observed the mass transfer of the electron [6] in multiple electron capture collisions of $F^{9+} + Ne$. These measurements were followed by the direct observation in the recoil momenta spectra of the signatures for the electron-electron and electron-nuclear interactions in $He^+, O^{7+} + He$ projectile ionization [7,8]. Unverzagt *et al.* at GSI [9] and Jardin *et al.* at Caen [10] then provided both longitudinal and transverse recoil momentum spectra for single and up to sevenfold ionization of Ne and Ar, which displayed the collective behavior of the ionized electrons. Very recently, Moshammer *et al.* have combined recoil ion and electron spectroscopy to perform the first *complete* momentum determination of the products in single ionization collisions for ion impact [11,12] and have clearly observed the importance of the electron-electron interaction in multiple ionization collisions [13]. [For a review of the numerous experimental investigations on kinematically complete $(e,2e)$ experiments for electron impact, see Ref. [14].] The French group at Caen [15] has made high precision state-selective electron capture measurements using recoil ion momentum spectroscopy for low-energy collisions involving $Ne^{10+}$ and $Ar^{18+}$, while the RIKEN group has performed similar investigations at much higher energies [16].

Presently, recoil ion momentum measurements made in coincidence with the projectile scattering angle measurements by Mergel *et al.* [17] illuminate the electron-electron Thomas mechanism for transfer ionization in $H^+ + He$ collisions, while Kravis *et al.* [18] have studied saddle-point electron production in low-energy collisions involving multiply charged ions. Furthering the development of the field is the investigation by Dörner *et al.* [19] who observed collision

 

plane information for slow electron production in 10- and 15-keV $H^+ + He$ collisions, and Tribedi *et al.* [20] who have obtained longitudinal momentum spectra for atomic and molecular hydrogen differential in the angle of the ejected electron.

Unfortunately, theoretical methods that describe the complete final state momentum information for single and multiple electron removal as a result of ion impact have not made the spectacular advances as those of the experimentalists. The major impediment is the lack of an *ab initio* quantal theory that can provide the coincidence information of all products for even the three-body single ionization reaction, let alone multiple ionization processes. In fact, there is only one *ab initio* quantal theory that includes electron correlation to accurately describe total cross sections for twofold ionization of the simplest many-electron target, the helium atom [21]. Conventional basis set expansion methods, while providing excellent accuracy for two-body interactions such as excitation and electron capture, are unable to provide momentum information for ionized electrons since the pseudostates used to represent the ionization channel do not have sufficient angular information. Only in the limit of high velocities for small perturbations where the first Born approximation is valid, has it been possible to include both the projectile-electron and the projectile-target nucleus interactions to obtain three-body kinematics [22–24]. With increasing perturbation strengths $q/v>1$, the dipole approximation breaks down and three-body interactions strongly influence the product state momentum balance. In much of this latter regime, the continuum distorted wave (CDW) method provides an accurate portrayal of postcollision and two-center collisional effects (see Ref. [25] for a review). In the CDW method, by invoking conservation of momentum and energy with the assumption that the recoil ion's energy is small compared to that of the electron and to the energy change of the projectile, accurate longitudinal momentum spectra for single ionization products can be obtained [26].

In order to fill the gap and provide interpretation and predictions of scattering dynamics, we have been lead to develop the $n$-body classical trajectory Monte Carlo (CTMC) method for single and multiple electron removal collisions [27]. In the CTMC method, the collision is evolved using classical mechanics, while the initial conditions contain necessary quantal information. A merit of the method is that all pairwise electron-nuclear and nuclear-nuclear interactions are included so that it is possible to provide a complete determination of the momenta of the product states of a collision, even for multiple ionization. In order to maintain parity with the experimental progress noted above, extensions have been made to the original CTMC method so that now model potentials based on Hartree-Fock calculations can be used to describe the electron-nuclear interactions [28], electrons on both target and projectile centers can be incorporated [7], dynamical screening of the nuclei during the collision may be included [29], and direct incorporation of the electron-electron interaction in the postcollision regime has been applied [13].

The motivation for the work reported here is to predict signatures of single ionization dynamics using coincidence procedures that are now within reach of experiment. The range of projectile charge state over collision speed $q/v$ is varied between 1.33 and 5.14. This is in contrast to a low perturbation strength $q/v=0.5$ study published for proton and antiproton collisions at 100 keV. In the latter, strong asymmetries in the collision plane for the antiproton case were predicted, and the impact parameter dependence for the formation of soft, saddle point, ECC, binary encounter, and backwards ejected electrons were illuminated [30]. These studies were recently extended to 300 and 500 keV to provide predictions [31] needed to design the recoil ion spectrometer for antiproton experiments conducted at the Low Energy Antiproton Ring in CERN. In the latter paper the electron longitudinal spectra for proton impact were compared to data from pioneering studies made using conventional electron spectroscopy methods [32].

## II. THEORETICAL METHOD

For a simple three-body collision system comprised of a fully stripped projectile (a), a bare target nucleus (b), and an active electron (c), the application of the CTMC method is relatively straightforward. One first writes down the classical Hamiltonian for the system

$$H=\frac{p_a^2}{2m_a}+\frac{p_b^2}{2m_b}+\frac{p_c^2}{2m_c}+V_{ab}(r_{ab})-\frac{Z_a}{r_{ac}}+V_{bc}(r_{bc}), \tag{1}$$

where $p_i$ are the momenta and $V_{ij}(r_{ij})$ are the pairwise interaction potentials between the individual particles. From Eq. (1), one obtains a set of 18-coupled, first-order differential equations arising from the necessity to determine the time evolution of the $xyz$ Cartesian coordinates of each particle,

$$\frac{dq_i}{dt}=\frac{\partial H}{\partial p_i} \tag{2}$$

and their corresponding momenta,

$$\frac{dp_i}{dt}=-\frac{\partial H}{\partial q_i}. \tag{3}$$

Five random numbers, constrained by $V_{bc}(r_{bc})$ and the binding energy of the target atom, are used to initialize the plane and eccentricity of the electron's orbit, and another is used to determine the impact parameter within the range of interaction. For our work, we utilize a fourth-order Runge-Kutta integration method because of its ease of use and its ability to vary the time step size. This latter requirement is essential since it is not uncommon for the time step to vary by three orders of magnitude during a single trajectory.

In essence, the CTMC method is a computer experiment. Total cross sections for a particular process are determined by

$$\sigma_R=\left(\frac{N_R}{N}\right)b_{\max}^2, \tag{4}$$

where $N$ is the total number of trajectories run within a given maximum impact parameter $b_{\max}$, and $N_R$ is the number of

positive tests for a reaction such as electron capture or ionization. Momentum differential cross sections are easily generalized from the above.

For single electron removal reactions with a He target atom, it is adequate to treat the problem within a one-electron model and employ the independent electron approximation to approximate atomic shell structure. For an accurate calculation, it is necessary to use an interaction potential that simulates the screening of the target nucleus by the electrons. One can simply apply a Coulomb potential with an effective charge $Z_{\mathrm{eff}}$, such as obtained from Slater's rules. Then, the computational procedure is the same as for a hydrogenic case. However, the boundary conditions for the long-range and short-range interactions are poorly satisfied.

To improve the electronic representation of the target, potentials derived from quantum-mechanical calculations were used. Here, the simple solution of Kepler's equation cannot be applied. However, Peach *et al.* [33] and Reinhold and Falcón [34] have provided the appropriate methods that yield a target representation that is correct under the microcanonical distribution. For our work, we employ the method of Reinhold and Falcón because of its ease of use and flexibility. Moreover, we have standardized our codes for a model potential of the form

$$V_{bc}(R)=\frac{-[Z_b-N_bS(R)]}{R} \tag{5}$$

with the screening of the core given by

$$S(R)=1-\left\{\left(\frac{\eta}{\xi}\right)[\exp(\xi R)-1]+1\right\}^{-1/2}. \tag{6}$$

In Eqs. (5) and (6), $Z_b$ and $N_b$ denote the nuclear charge and number of nonactive electrons in the target core, and $\eta$ and $\xi$ are screening parameters.

The major reason for our choice of this interaction potential is that Garvey *et al.* [35] have performed a large set of Hartree-Fock calculations and have parametrized their results in the above functional form. Screening parameters are given for all ions and atoms for $Z\leqslant 54$. This potential can also be used for the representation of partially stripped projectile ions. Moreover, in order to predict spectra differential in the momentum of all outgoing particles, it is necessary that all interaction potentials are accurate in both the united and separated atom limits.

## III. RESULTS

### A. Longitudinal momentum spectra

In order to illustrate the collision dynamics as a function of perturbation strength $q/v$, we will concentrate on 9.5-MeV/nucleon $Ni^{26+}$ and 3.6-MeV/nucleon $Se^{28+}$ single ionization collisions with He. Here, the $q/v$ values are 1.33 and 2.34, respectively. Moreover, there are complete experimental momentum spectra for these two systems with which to compare the calculational results. These measurements were made at GSI Darmstadt by the authors using the experimental setup recently described in Ref. [12]. Since the perturbation strength cannot completely specify a system, we will contrast these results with those of 506- and 165-keV/nucleon $C^{6+}$, which have the same $q/v$ values. As will be shown, the 165-keV/nucleon $C^{6+}$ spectra are especially rich because electron capture is a major component of the electron removal processes, in turn, this strongly affects the three-body ionization spectra. Finally, lest we begin to feel that the collision dynamics are well understood, we will compare the CTMC results to the 34-, 48-, and 66-keV/nucleon $C^{6+}+He$ longitudinal momentum spectra of Kravis *et al.* [18], which have $q/v$ values of 5.14, 4.33, and 3.69, respectively. Here, electron capture dominates over ionization and the agreement between experiment and theory is poor.

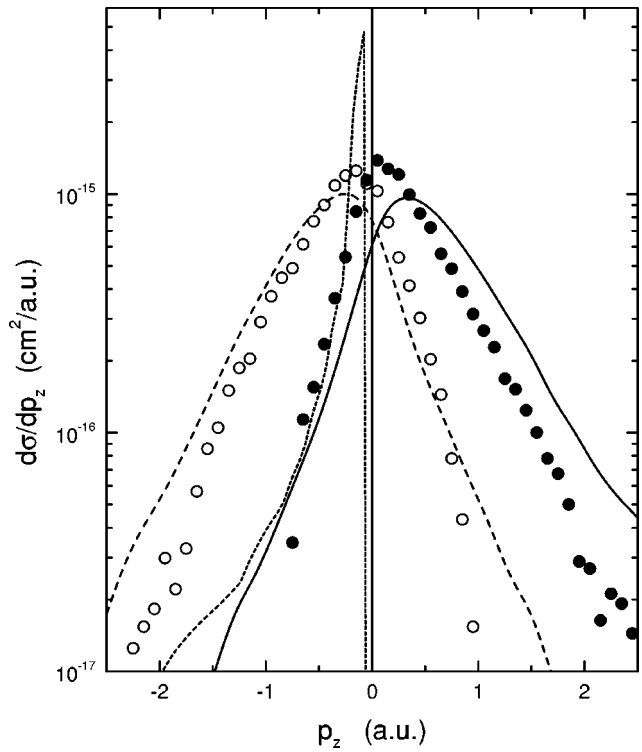


FIG. 1. Longitudinal momentum spectra for single ionization 9.5-MeV/nucleon $Ni^{26+}+He$ collisions. Our experimental electron and recoil ion spectra are given by filled and open circles, respectively. The CTMC values for the electron and recoil ion spectra are given by the solid and long-dashed line, respectively. The theoretical change in longitudinal momentum of the projectile is given by the short-dashed line. The CTMC cross sections have been multiplied by a factor of 2.41 to the experimental value of $2.6\times 10^{-15}\mathrm{cm}^2$.

In Fig. 1 our experimental and theoretical results are presented for the 9.5-MeV/nucleon $Ni^{26+}$ system, where $q/v=1.33$. The CTMC values, which are known to underestimate the total ionization cross sections at high energies because of the poor classical description of large impact parameter collisions that give rise to slow electrons, have been normalized to the experimental results. In turn, the experimental data are absolutely normalized by extrapolating the absolute data of Berg *et al.* [36], which are accurate to $\pm 30\%$. For the recoil ion spectra, there is reasonable overall agreement between theory and experiment with the maximum value of the longitudinal momentum found at $-0.2$ a.u. The calculated electron spectra are found to peak at approximately 0.3 a.u. The forward shift is due to the post-

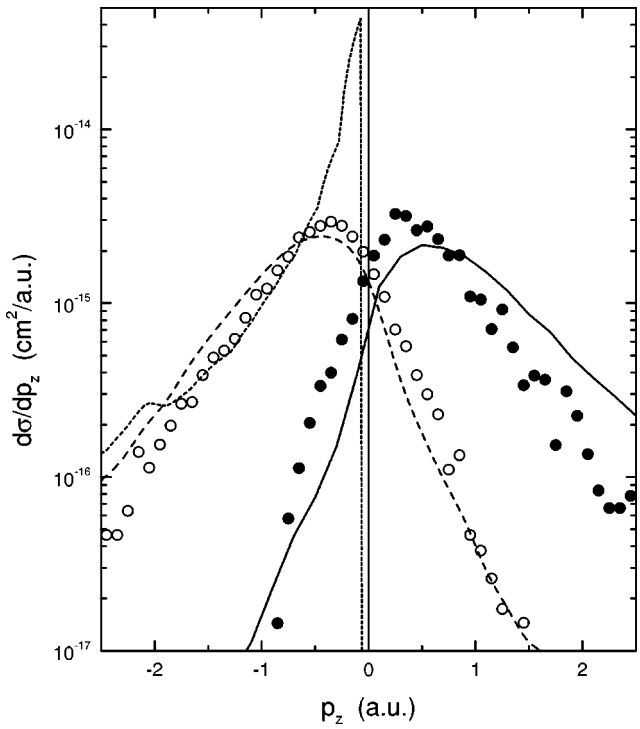


FIG. 2. Longitudinal momentum spectra for 3.6-MeV/nucleon $Se^{28+}$+He single ionization collisions. The notation is the same as that in Fig. 1. Here, the CTMC cross sections have been multiplied by a factor of 1.38 to the experimental value of $3.3\times10^{-15}$ cm$^2$.

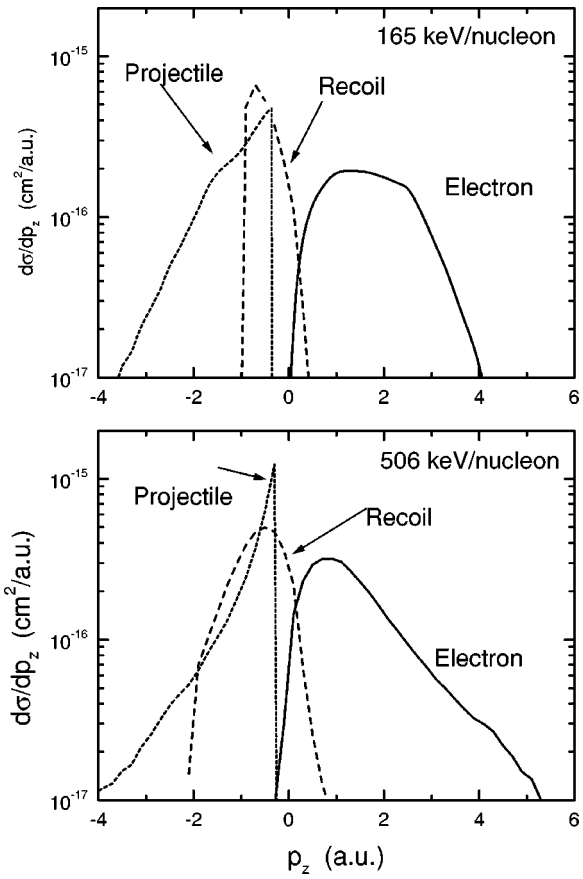


FIG. 3. Calculated values for the longitudinal momentum spectra for $C^{6+}$+He at 165 and 506 keV/nucleon. The electron and recoil ion spectra are given by solid and long-dashed lines, while the change in momentum of the projectile is given by the short-dashed line.

collision interaction with the highly charged projectile. The asymmetry between the recoil and electron longitudinal momentum, with the electrons having a larger cross section at positive values of the longitudinal momentum than the corresponding values at negative momenta for the recoil ion, is caused by the momentum change of the projectile, which can only be negative. The calculated momentum change of the projectile is also given in Fig. 1. The loss of projectile momentum is very sharply peaked with the maximum occurring at $Q/v=-0.046$ a.u., the value that corresponds to zero energy ionized electrons. The experimental electron spectra indicate that the electrons are more backwardly scattered than given by the calculations, with a maximum value at $p_z \approx 0.1$ a.u. As a check we have verified that the full three-body calculations are preserving conservation of momentum and energy.

As the perturbation strength is increased to $q/v=2.34$ for the 3.6-MeV/nucleon $Se^{28+}$ system, the overall trends of the longitudinal momentum spectra remain similar to that for the 9.5-MeV/nucleon $Ni^{26+}$ case. The calculated and experimental recoil ion spectra are again in good agreement with one another, and are found to maximize at approximately $-0.4$ a.u., Fig. 2. The same disagreement as before exists for the electron spectra. Here the calculations maximize at approximately 0.55 a.u., while the experimental value is around 0.3 a.u. For the CTMC results, the asymmetry in the recoil ion versus the electron spectra is further enhanced in comparison to the 9.5-MeV/nucleon results. This is because the projectile momentum loss broadens considerably as the speed of the projectile decreases. As expected, the change in projectile momentum is negative, and is found to peak at a $Q/v$ value of $-0.075$ a.u.

The 3.6-MeV/nucleon $Se^{28+}$ system is very similar to the 3.6-MeV/nucleon $Ni^{24+}$ system that was studied previously [11]. In that work, there was good agreement between $n$-CTMC calculations and the experiment in the peak positions of the recoil ion, and electron longitudinal momenta. A series of continuum distorted wave calculations have been recently carried out for the $Ni^{24+}$ system, where good agreement has been demonstrated for the absolute cross sections [37]. These calculations tended to underestimate the forward shift of the electron, and backward shift of the recoil ion, spectra. The authors stated that this discrepancy with experiment and CTMC calculations may be due to the neglect of the nuclear-nuclear distortion in the calculations.

It is illustrative to consider another collision system and investigate the momentum spectra at the same values of perturbation strength as those used above. For this comparison, we have used $C^{6+}$ at an energy of 506 keV/nucleon ($q/v=1.33$) and 165 keV/nucleon ($q/v=2.34$). Their longitudinal momentum spectra are given in Fig. 3. For both cases the projectile momentum loss is found to significantly influence the three-body spectra, and has a width that approaches (506 keV/nucleon) and even exceeds (165 keV/nucleon) that of the recoil ion.

The 165-keV/nucleon $C^{6+}$ case differs greatly from the 3.6-MeV/nucleon $Se^{28+}$ collision system mainly because it is influenced by electron capture, which is not appreciable for

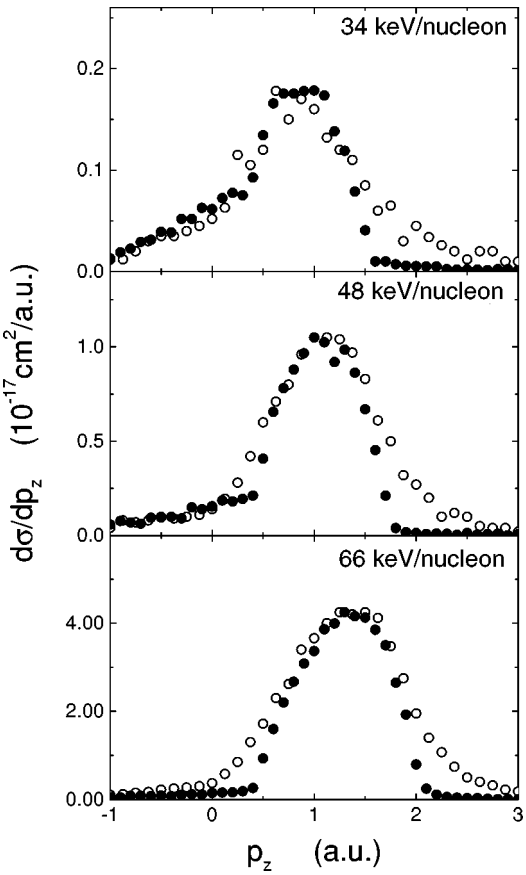


FIG. 4. Longitudinal electron momentum spectra for 34-, 48-, and 66-keV/nucleon $C^{6+}+He$. The data of Kravis *et al.* [18] are given by the open circles. The CTMC calculations are given by the filled circles. Note that the CTMC results have been shifted to more positive values of $p_z$ by a constant 0.4 a.u. at each energy.

the higher-energy $Se^{28+}$. This is apparent from several characteristics, one of which is the electron-capture-to-the-continuum (ECC) shoulder on the electron spectrum that occurs at the projectile speed of 2.57 a.u. A complementary shoulder is also apparent on the projectile momentum loss distribution at $-1.63$ a.u. The onset of electron capture is also displayed in the recoil ion momentum, in that a sharp cutoff in momentum is found at $-0.93$ a.u. This value corresponds to the ECC process, with recoil momenta at more negative values being discrete, and corresponding to electron capture to the ground and excited states of $C^{5+}$.

Experimental electron longitudinal momentum spectra exist for $C^{6+}+He$ collisions at 66, 48, and 34 keV/nucleon ($q/v=3.69$, 4.33, and 5.14, respectively). In Fig. 4, the comparison between CTMC results and the measurements of Kravis *et al.* [18] are displayed. Here, even though the CTMC calculations very nicely reproduced the out-of-plane component of the ionized electron spectra (Fig. 7 of Ref. [18]), the longitudinal momenta differ considerably. Note that the CTMC results have been shifted by a constant $+0.4$ a.u. in each case. With this shift, the widths of the longitudinal spectra are in accord with one another. To verify that the calculations were encompassing the ECC component of the ionized electrons, the integration routine was changed to follow each ECC event to $10^7$ a.u., or 0.5 mm, past the collision center. Thus, the lack of a strong component of ECC electrons in the calculations could not be reconciled. Moreover, we have calculated the state selective electron capture cross sections for these systems, since it is possible to Stark ionize high $C^{5+}$ Rydberg states in the deflector plates of the experiment. However, we find the $C^{5+}$ electron capture distributions narrowly peaked about $n=3-4$, with insufficient high $n$ values needed to reconcile the difference with experiment.

A process that may explain the difference is the double excitation channel. This process is not included in our one-electron calculations, but will give rise to ~35-eV electrons ($v\approx 1.60$ a.u.) with a cross section that is approximately 1 $-10\%$ of the total ionization value. Such a reaction yields a $He^+$ recoil ion, as detected in the coincidence measurement. Moreover, these electrons will reside in the cusp region of the electron spectra, and may be further focused to this area by the slow highly charged $C^{6+}$ projectile. Further work on this topic will be required.

To investigate the possibility of a clear signature of ECC or saddle point electrons in the electron longitudinal momentum spectra, calculations for $H^+$ and $C^{6+}$ projectiles have been carried out for collision speeds of 1 to 12 a.u. The relative peak positions $v^*=v_{\max}^{\mathrm{el}}/v_{\mathrm{proj}}$, where $v_{\max}^{\mathrm{el}}$ is the maximum in the longitudinal velocity distribution of the emitted electron and $v_{\mathrm{proj}}$ is the projectile velocity, were then plotted as a function of projectile speed. In such a plot the ECC electrons occur at $v^*=1$, and saddle-point electrons are located at $v^*=[1+(q_p/q_t)^{1/2}]^{-1}$, where $q_p$ is the final projectile charge and $q_t$ is the final target charge. The results are inconclusive; see Fig. 5. At high speeds, the longitudinal force induced by the projectile on the ionized electron balances to zero, with the transverse force causing most electrons to be ejected around 90° with a $p_z$ value close to zero. As the collision energy is lowered, two-center effects become more prominent with the longitudinal momentum maximizing near the saddle point velocity at calculated values of 1.9 a.u. for $H^+$ (90 keV), and 3.6 a.u. for $C^{6+}$ (325 keV/nucleon). Interestingly, within statistical errors the CTMC calculations tend to a maximum, then decrease toward the saddle-point velocity at very low collision speeds. This behavior is also demonstrated in the CDW calculations of Fainstein [26] and is borne out by the measurements of Kravis *et al.*, which show a similar behavior for $C^{6+}$, but are inconclusive for $H^+$.

### B. Collision plane studies

A major attribute of the momentum spectroscopy method is that it is now possible to perform collision plane studies that more fully elucidate the various scattering mechanisms. In the data presented here, we will use a collision plane defined by the incident projectile momentum ($+z$ coordinate) and the outgoing transverse momentum of the recoil ion ($+x$ coordinate). This is a collision plane that is most amenable to the experimental setup, since there is no direct measurement on the outgoing projectile at these energies. At lower energies where it is feasible to measure the projectile deflection it will be possible to use a collision plane defined by the projectile scattering. Either coordinate system can be utilized in the calculations since all nine final-state momentum components are determined.

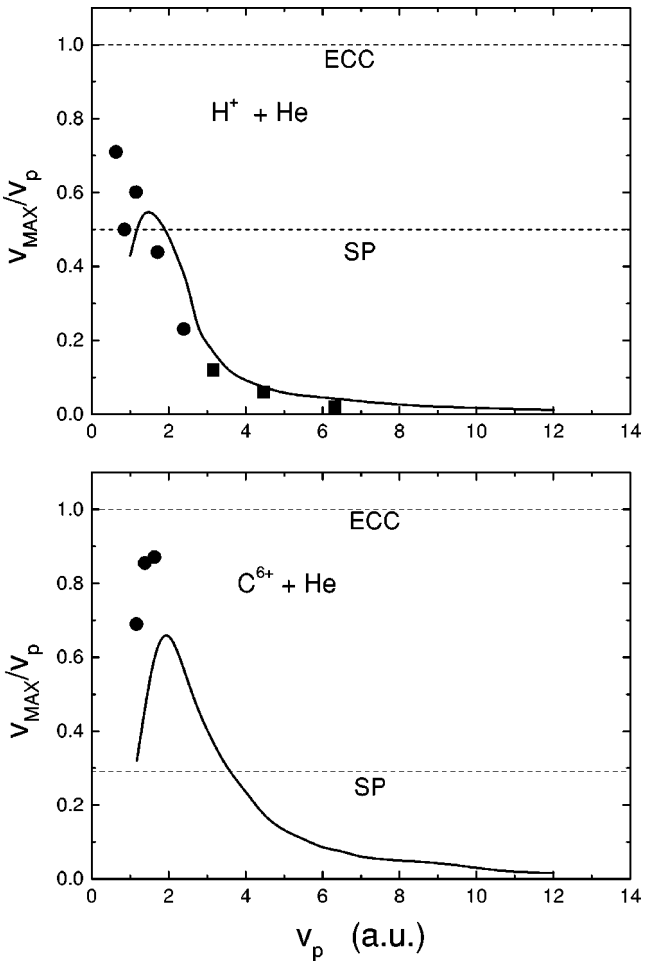


FIG. 5. Energy dependence of the position of the maximum in the electron longitudinal momentum $v_{\max}^{\mathrm{el}}$ as a function of projectile speed $v_p$. The reduced function $v_{\max}^{\mathrm{el}}/v_p$ for the ordinate is used so that the ECC position is constant at unity. Likewise, the position of the saddle point velocity SP is given for the two systems under consideration. The CTMC calculations for $H^+$ and $C^{6+}$+He are shown by the solid line. Experimental data from Kravis *et al.* [18] and Dörner *et al.* [38] are denoted by solid circles and squares, respectively.

In Fig. 6 theoretical results for 9.5-MeV/nucleon $Ni^{26+}$ are shown, and in Fig. 7 the comparison between theory and experiment is given for the 3.6-MeV/nucleon $Se^{28+}$ system. Here, the $x$ and $z$ momentum components for all the reaction products of each ionizing collision are presented. The overall general trends are well reproduced by the calculations. However, differences are apparent in that the calculated transverse momentum components of the recoil ion and ionized electron are more broadly distributed than in the $Se^{28+}$ experimental observations, with the ionized electrons more likely to be scattered in an azimuthal direction opposite to that of the recoil ion. The change in momentum for the projectile is relatively sharp, with the calculations being more highly peaked than the experiment. The experimental determination of the projectile loss is deduced from the coincident observation of the recoil ion and ionized electron, and is effected by finite resolution, so this difference is not considered significant.

Even though the perturbation strengths for 3.6-MeV/nucleon $Se^{28+}$ and 165-keV/nucleon $C^{6+}$ are identical, the

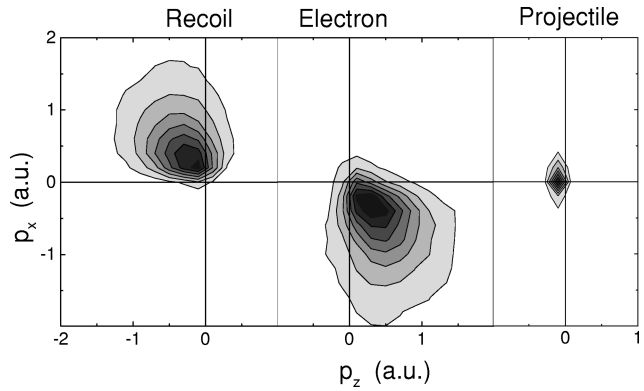


FIG. 6. Calculated three-body momentum spectra for 9.5-MeV/nucleon $Ni^{26+}$+He single ionization collisions. The collision plane is defined by the incident projectile momentum, and the transverse momentum of the outgoing recoil ion. The $x$- and $z$-momentum components of the collisions products are presented. The plots are made using a linear scale where each contour line represents an equal portion of the cross section.

$C^{6+}$ system differs significantly from $Se^{28+}$ when one considers the collision plane information. In Fig. 8 the electron spectra are presented for electrons just in the projectile-recoil collision plane. Here, we have restricted the $y$ component of electron momentum to be less than 0.05 a.u. In the upper left figure, all counts are given with no other restrictions. The spectrum is asymmetric with the electrons being preferentially emitted opposite to the recoil ion. Local maxima are present for the slow electrons and the ECC electrons. The ECC electrons have the known asymmetry to smaller values of $p_z$ around the cusp at the projectile velocity. They are also

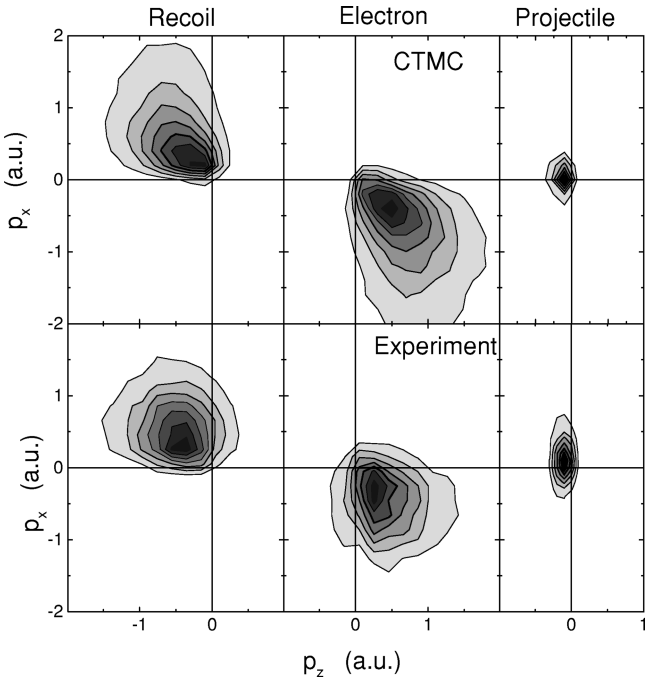


FIG. 7. Calculated and experimental three-body momentum spectra for 3.6-MeV/nucleon $Se^{28+}$+He single ionization collisions. The experimental projectile change momenta are deduced from the coincident observation of the momenta of the ionized electron and recoil ion. Notation is the same as in Fig. 6.

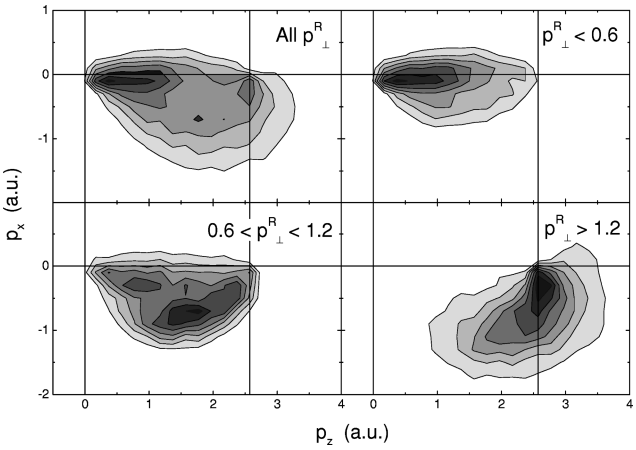


FIG. 8. Calculated electron collision plane results for the 165-keV/nucleon $C^{6+}$+He system. Here, the spectra are coincident with electrons whose perpendicular momentum components are between $\pm 0.05$ a.u. The upper left figure has all recoil ion transverse momenta counts. For soft collisions, the upper right figure restricts the transverse momentum of the recoil ion to be less than 0.6 a.u. Intermediate collisions are given in the lower left figure, while hard collisions with recoil transverse momenta greater than 1.2 a.u. are in the lower right figure. The ranges of the transverse momentum of the recoil ion were chosen so that each of the three latter figures represented an equal portion of the total cross section.

found to be very asymmetric in the $p_x$ plane with the ECC electrons being preferentially emitted at an azimuthal angle of 180° from the recoil ion.

In order to follow the collision dynamics further, the upper left spectrum has been cut in terms of the transverse momentum of the recoil ion. By so doing, small transverse recoil ion momenta roughly correspond to large impact parameters, and large transverse momenta relate to the more violent small impact parameter collisions. Each of the three coincident spectra given in Fig. 8 contribute equally to the total cross section. For small recoil transverse momenta, i.e., large impact parameters, primarily slow electrons are formed (upper right figure). In this case, there is a slight tendency for the electrons to be produced azimuthally opposite to the recoil ion in the projectile's direction. For intermediate collisions (lower left figure), considerable two-center electrons are produced with a significant tendency for the electrons to be emitted opposite to the recoil ion. This behavior is even more accentuated for the hard collisions with large recoil transverse momenta (lower right figure). Electrons around the ECC cusp now dominate. It is significant that these electrons are found to have an almost complete asymmetry in the collision plane with azimuthal angles opposite to that of the recoil ion, and with that of the projectile. Such an asymmetry is very surprising because the projectile scattering is on the order of tens of microradians, while the electron asymmetry is on the order of tens of degrees. From this, one would infer that these ECC electrons not only have the known asymmetry in energy about the cusp, but are also strongly polarized in the projectile scattering plane.

### C. Azimuthal angle dependence

A convenient way to follow the angular correlation in the three products of the single ionization reaction is to plot the

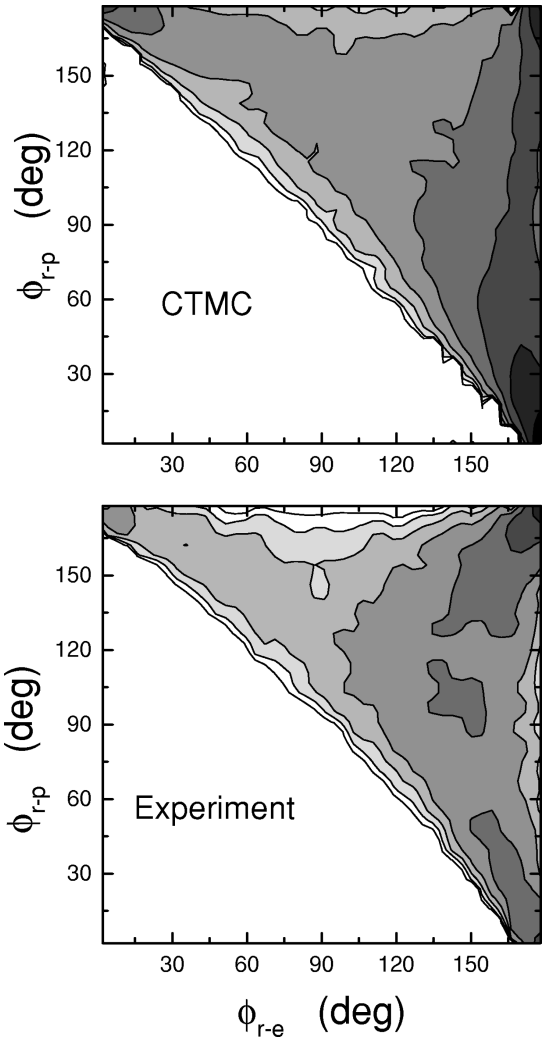


FIG. 9. Azimuthal angle dependencies between the recoil ion and ionized electron, abscissa, and recoil ion and projectile, ordinate, for the 9.5-MeV/nucleon $Ni^{26+}$ system. The CTMC results are in the upper figure and the experimental values in the lower figure. A logarithmic scale was used for the eight contour lines.

azimuthal angle between the projectile and recoil ion versus that of the recoil ion and ionized electron. For small impact parameter or low-energy collisions, there will be a strong 180° correlation between the recoil ion and projectile, with the counts appearing along the top horizontal section of the plot. For large impact parameter or high energy collisions, the projectile transfers energy to ionize the target but does not appreciably participate in the postcollision momentum sharing. For these cases, the recoil ion and electron ionize back-to-back with a 180° correlation between each other where the counts appear along the right-hand vertical portion of the graph. If there is a hard collision between the projectile and electron so that binary electron production occurs, the projectile and ionized electron will scatter at 180° to each other and the counts will appear along the diagonal portion of the graph.

In Fig. 9 the 9.5-MeV/nucleon $Ni^{26+}$ system is investigated. The CTMC calculations portray the general aspects of these collisions with most of the counts found along the vertical section which reflects momentum sharing between the recoil ion and ionized electron. In such fast collisions there is

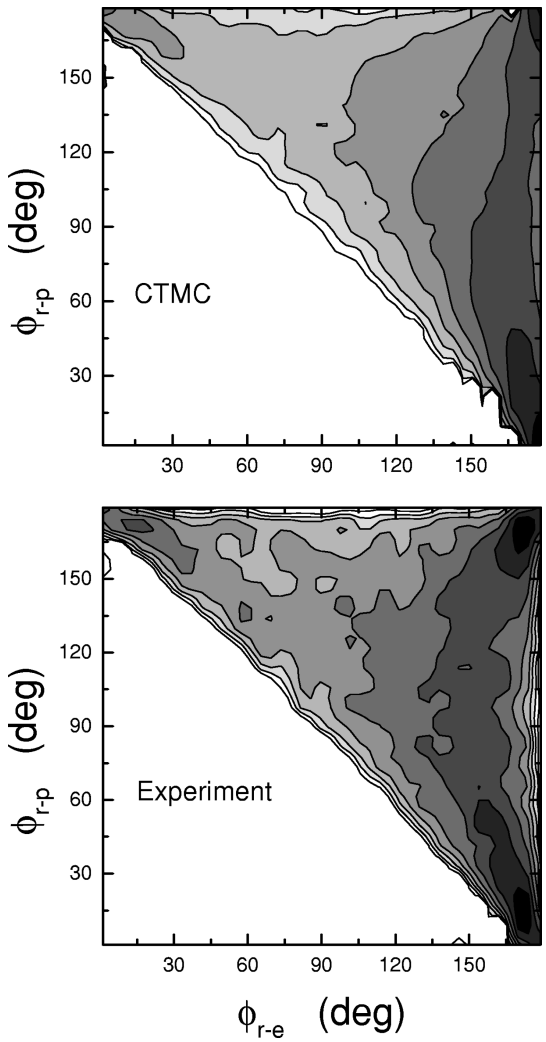


FIG. 10. Azimuthal angle dependencies for the 3.6-MeV/nucleon $Se^{28+}$ system. The notation is the same as in Fig. 9.

very little change in momentum of the projectile, so that the target products primarily explode back-to-back. We do note that the measurements indicate that the correlation between the ionized electron and recoil ion is somewhat more diffuse than that calculated. Interestingly, both experiment and theory display a small island of counts in the upper left section of the plots where there is a 180° correlation between recoil ion and projectile along with a near 0° correlation between recoil ion and electron. These events occur in relatively small impact parameter collisions where the projectile, at its distance of closest approach, passes between the recoil ion and ionized electron. The transverse impulse given to products causes the positively charged projectile and recoil ion to repel one another, while the electron is attracted toward the projectile. After the collision, the projectile's transverse momentum is then found to be balanced by the sum of that of the recoil ion and ionized electron.

The azimuthal angle dependencies for the 3.6-MeV/nucleon $Se^{28+}$ are very similar to that of $Ni^{26+}$, Fig. 10. Again theory yields a sharper pattern than that of the experiment, with a dominance of recoil ion–ionized electron back-to-back scattering. Both theory and experiment show a strong maximum in the lower right hand corner where the recoil ion and electron are at 180° to one another, and the

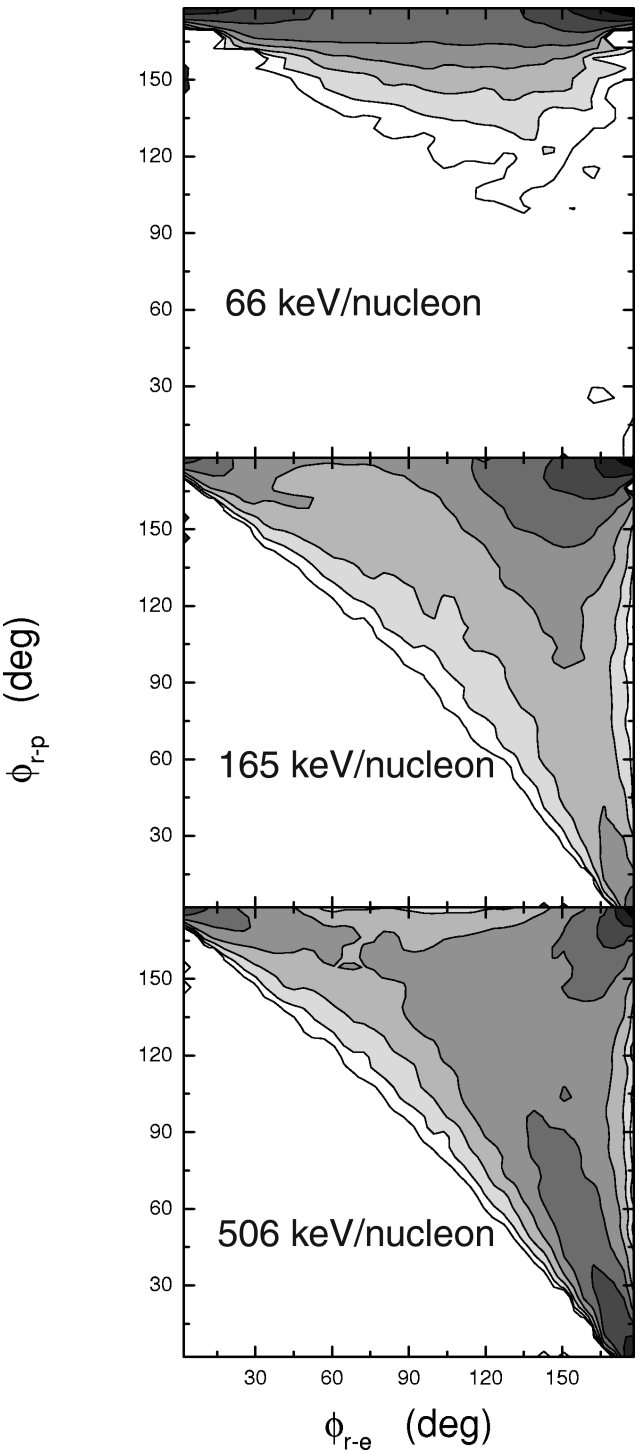


FIG. 11. Calculated azimuthal angle dependencies for the $C^{6+}$ system at 66, 165, and 506 keV/nucleon. Notation is the same as in Fig. 9.

projectile, and recoil ion are near 0°. Analysis of the CTMC results indicate that these are primarily large impact parameter collisions where the electron's transverse momentum is balanced by the transverse momenta of the projectile, which is attracted toward the electron at the distance of closest approach and that of a very low momentum recoil ion, which partially absorbs some of the deflection of the projectile.

To study the evolution of azimuthal angle dependencies, calculations are presented for $C^{6+}$ at 66, 165, and 506 keV/

nucleon, Fig. 11. These energies correspond to perturbation strengths $q/v$ of 3.69, 2.34, and 1.33, respectively. For the largest perturbation strength corresponding to 66 keV/nucleon, two-body heavy particle nuclear scattering dominates, with the ionized electron having little effect on the transverse momentum balance (top figure). At the intermediate energy of 165 keV/nucleon, the electron becomes an equal partner in the momentum balance with three local maxima apparent in the three corners of the azimuthal angle correlations (middle figure). As the collision energy is further increased to 506 keV/nucleon, the projectile contributes a minor fraction to the transverse momentum balance with this now controlled by the back-to-back explosion between the recoil ion and ionized electron, lowest figure.

## IV. CONCLUDING REMARKS

The field of momentum spectroscopy has matured rapidly in just the last several years. This progress now makes it possible to perform kinematically complete experiments and calculations for single ionization collisions induced by ion impact. Such studies provide insight into the dynamics and momentum sharing of three-body reactions.

In this paper we concentrated on large perturbation strength collisions where the charge state of the projectile divided by collision speed $q/v$ was greater than unity. In general, the $q/v$ parameter characterized many of the momentum spectra. However, the presence of a strong electron capture channel leads to rich structure displaying soft, two-center, and ECC electrons at lower velocities. Collision plane studies differential in the transverse momentum of the recoil ion provide a method to separately probe soft collisions where the recoil ion momentum is small, to those involving small impact parameter violent collisions where the recoil ion momentum is large. Such studies, when combined with the azimuthal angle dependencies between the three reaction products, leads to an improved understanding of ionization collisions.

Many detailed questions arise when direct comparisons are made between theoretical calculations and experimental data. Since the CTMC method incorporates all the pairwise Coulomb forces between the particles for a three-body single ionization reaction, it is possible to do a kinematically complete calculation. This has not been feasible by any quantal method that is applicable to the collision systems presented here. However, the many discrepancies between theory and experiment indicate that further theoretical development is needed.

In particular, there is notable disagreement between theory and experiment for the very strong perturbation strength 34–64-keV/nucleon $C^{6+}+He$ collisions. Here, CTMC calculations underestimate the position of the maxima in the longitudinal electron spectra, while CDW results overestimate its position and the width of the transverse spectra [39]. Both of these methods are three-body theories, which probably infers that a more complete four-body study of this system is necessary.

As pointed out in this paper and in Ref. [31], probably the most interesting systems of study will be those at intermediate energies such as 165-keV/nucleon $C^{6+}+He$. Here, the electron capture and ionization channels are both equally important, giving rise to nice illustrations of soft, saddle-point, and cusp electron dynamics. The experimental studies to present have primarily concentrated on either relatively high energy MeV/nucleon collisions, or those below 100 keV/nucleon where electron capture dominates. Further experiments in this area from the Kansas State and Freiburg laboratories are now under way.

## ACKNOWLEDGMENTS

The authors would like to thank the Office of Fusion Research of the Department of Energy, GSI, the Deutsche Forschungsgemeinschaft, the Bundesministerium für Bildung und Forschung, and the Alexander von Humboldt Stiftung for their support.

[1] C. L. Cocke and R. E. Olson, Phys. Rep. **205**, 153 (1991).
[2] J. Ullrich, R. Moshammer, R. Dörner, O. Jagutzki, H. Schmidt-Böcking, and L. Spielberger, J. Phys. B **30**, 2917 (1997).
[3] R. Dörner, J. Ullrich, H. Schmidt-Böcking, and R. E. Olson, Phys. Rev. Lett. **63**, 147 (1989).
[4] R. Ali, V. Frohne, C. L. Cocke, M. Stockli, S. Cheng, and M. L. A. Raphaelian, Phys. Rev. Lett. **69**, 2491 (1992).
[5] W. Wu, J. P. Giese, I. Ben-Itzhak, C. L. Cocke, P. Richard, M. Stockli, R. Ali, H. Schöne, and R. E. Olson, Phys. Rev. A **48**, 3617 (1993).
[6] V. Frohne, S. Cheng, R. Ali, M. Raphaelian, C. L. Cocke, and R. E. Olson, Phys. Rev. Lett. **71**, 696 (1993).
[7] R. Dörner, V. Mergel, R. Ali, U. Buck, C. L. Cocke, K. Froschauer, S. Lencinas, W. E. Meyerhof, S. Nüttgens, R. E. Olson, H. Schmidt-Böcking, L. Spielberger, K. Tökesi, J. Ullrich, M. Unverzagt, and W. Wu, Phys. Rev. Lett. **72**, 3166 (1994).
[8] W. Wu, K. L. Wong, R. Ali, C. L. Cocke, V. Frohne, J. P. Giese, M. Raphaelian, B. Walch, R. Dörner, V. Mergel, H. Schmidt-Böcking, and W. E. Meyerhof, Phys. Rev. Lett. **72**, 3170 (1994).
[9] M. Unverzagt, R. Moshammer, R. E. Olson, P. Jardin, V. Mergel, J. Ullrich, and H. Schmidt-Böcking, Phys. Rev. Lett. **76**, 1043 (1996).
[10] P. Jardin, A. Cassimi, J. P. Grandin, D. Hennecart, and J. P. Lemoigne, Nucl. Instrum. Methods Phys. Res. B **107**, 41 (1996).
[11] R. Moshammer, J. Ullrich, M. Unverzagt, W. Schmitt, P. Jardin, R. E. Olson, R. Mann, R. Dörner, V. Mergel, U. Buck, and H. Schmidt-Böcking, Phys. Rev. Lett. **73**, 3371 (1994).
[12] R. Moshammer, J. Ullrich, H. Kollmus, W. Schmitt, M. Unverzagt, H. Schmidt-Böcking, C. J. Wood, and R. E. Olson, Phys. Rev. A **56**, 1351 (1997).
[13] R. Moshammer, J. Ullrich, H. Kollmus, W. Schmitt, M. Unverzagt, O. Jagutzki, V. Mergel, H. Schmidt-Böcking, R. Mann, C. J. Wood, and R. E. Olson, Phys. Rev. Lett. **77**, 1242 (1996).

[14] A. Lahmam-Bennani, J. Phys. B **24**, 2401 (1991).
[15] A. Cassimi, S. Duponchel, X. Flechard, P. Jardin, P. Sportais, D. Hennecart, and R. E. Olson, Phys. Rev. Lett. **76**, 3679 (1996).
[16] T. Kambara, A. Igarashi, N. Watanabe, Y. Nakai, T. M. Kojima, and Y. Awaya, J. Phys. B **30**, 1251 (1997).
[17] V. Mergel *et al.*, Phys. Rev. Lett. **79**, 387 (1997).
[18] S. D. Kravis, M. A. Abdallah, C. L. Cocke, C. D. Lin, M. Stockli, B. Walch, Y. D. Wang, R. E. Olson, V. D. Rodriguez, W. Wu, M. Pieksma, and N. Watanabe, Phys. Rev. A **54**, 1394 (1996).
[19] R. Dörner, H. Khemliche, M. H. Prior, C. L. Cocke, J. A. Gary, R. E. Olson, V. Mergel, J. Ullrich, and H. Schmidt-Böcking, Phys. Rev. Lett. **77**, 4520 (1996).
[20] L. C. Tribedi, P. Richard, Y. D. Wang, C. D. Lin, and R. E. Olson, Phys. Rev. Lett. **77**, 3767 (1996).
[21] J. F. Reading and A. L. Ford, J. Phys. B **20**, 3747 (1987).
[22] A. Salin, J. Phys. B **22**, 3901 (1989).
[23] X. Fang and J. F. Reading, Nucl. Instrum. Methods Phys. Res. B **53**, 453 (1991).
[24] H. Fukuda, I. Shimamura, L. Vegh, and T. Watanabe, Phys. Rev. A **44**, 1565 (1991).
[25] N. Stolterfoht, R. D. DuBois, and R. D. Rivarola, *Electron Emission in Heavy Ion-Atom Collisions* (Springer-Verlag, Berlin, 1997).
[26] P. D. Fainstein, J. Phys. B **29**, L763 (1996).
[27] R. E. Olson, J. Ullrich, and H. Schmidt-Böcking, Phys. Rev. A **39**, 5572 (1989).
[28] D. R. Schultz, C. O. Reinhold, and R. E. Olson, Phys. Rev. A **40**, 4947 (1989).
[29] V. J. Montemayor and G. Schiwietz, Phys. Rev. A **40**, 6223 (1989).
[30] C. J. Wood and R. E. Olson, J. Phys. B **29**, L257 (1996).
[31] R. E. Olson, C. R. Feeler, C. J. Wood, C. L. Cocke, R. Dörner, V. Mergel, H. Schmidt-Böcking, R. Moshammer, and J. Ullrich, Nucl. Instrum. Methods Phys. Res. B **124**, 249 (1997).
[32] M. E. Rudd, L. H. Toburen, and N. Stolterfoht, At. Data Nucl. Data Tables **18**, 413 (1976).
[33] G. Peach, S. L. Willis, and M. R. C. McDowell, J. Phys. B **18**, 3921 (1985).
[34] C. O. Reinhold and C. A. Falcón, Phys. Rev. A **33**, 3859 (1986).
[35] R. H. Garvey, C. H. Jackman, and A. E. S. Green, Phys. Rev. A **12**, 1144 (1975).
[36] H. Berg, J. Ullrich, E. Bernstein, M. Unverzagt, L. Spielberger, J. Euler, D. Schardt, O. Jagutzki, H. Schmidt-Böcking, R. Mann, P. H. Molker, S. Hagmann, and R. D. Fainstein, J. Phys. B **25**, 3655 (1992).
[37] S. F. C. O'Rourke and D. S. F. Crothers, J. Phys. B **30**, 2443 (1997).
[38] R. Dörner, V. Mergel, L. Zhaoyuan, J. Ullrich, L. Speilberger, R. E. Olson, and H. Schmidt-Böcking, J. Phys. B **28**, 435 (1995).
[39] M. Abdallah, S. Kravis, C. L. Cocke, Y. Wang, V. D. Rodriguez, and M. Stöckli, Phys. Rev. A **56**, 2000 (1997).